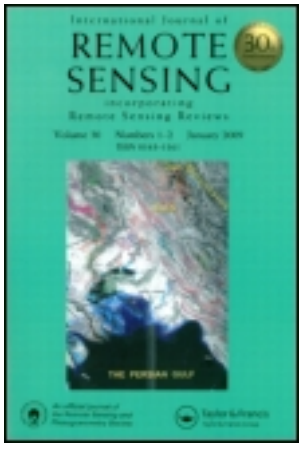

International Journal of Remote Sensing

Publication details, including instructions for authors and subscription information:
http://www.tandfonline.com/loi/tres20

Comparison of methods for melt detection over Greenland using active and passive microwave measurements

Ivan S. Ashcraft [a] & David G. Long [a]

[a] Brigham Young University, Microwave Earth Remote Sensing Laboratory

Published online: 22 Feb 2007.

To cite this article: Ivan S. Ashcraft & David G. Long (2006): Comparison of methods for melt detection over Greenland using active and passive microwave measurements, International Journal of Remote Sensing, 27:12, 2469-2488

To link to this article: http://dx.doi.org/10.1080/01431160500534465

International Journal of Remote Sensing
Vol. 27, Nos. 12–14, July 2006, 2469–2488

Taylor & Francis
Taylor & Francis Group

Comparison of methods for melt detection over Greenland using active and passive microwave measurements

IVAN S. ASHCRAFT and DAVID G. LONG*
Brigham Young University, Microwave Earth Remote Sensing Laboratory

(*Received 30 May 2005; in final form 13 December 2005*)

Microwave measurements have been used in various studies to detect melt based on their sensitivity to liquid water present in snow. To contrast different melt detection methods used with different sensors, six different melt detection method/sensor combinations are compared using data for the summer of 2000. The sensors include the Special Spectral Microwave Imager (SSM/I), SeaWinds on QuikSCAT (QSCAT), and the European Remote Sensing (ERS) Advanced Microwave Instrument (AMI) in scatterometer mode. Existing melt detection methods are compared with melt detection based on a simple physical model. The model relates the moisture content and depth of a surface melt layer of wet snow to a single channel melt detection threshold. The model can be applied to both active and passive sensors and improves the consistency between brightness temperature (T_b) and normalized radar backscatter (σ°) based detection of melt. Model-based melt estimates from different sensors are highly correlated and do not exhibit the unnatural phenomenon observed with previous methods. Relative merits and limitations of the various methods are discussed.

1. Introduction

The Greenland ice-sheet is an important factor in global sea level change, the Earth's radiation budget, and other areas of global environmental concern. Measuring the melt occurring each year on the ice-sheet is important in understanding climate and the Greenland mass balance. Approximately 8% of the world's ice is located on the Greenland ice-sheet with melting from the ice-sheet estimated to contribute 7% to the current rise in sea level (Krabill *et al.*, 2000). In relation to the Earth's radiation budget, rising temperatures cause increased melt extent. Even small temperature changes can affect large areas due to the shallow slope of the ice-sheet. Wet snow absorbs approximately 45% more incoming solar radiation than dry snow (Abdalati and Steffen, 1995). This increase in absorbed radiation with increasing temperatures represents unstable positive feedback in our climate.

Microwave measurements of brightness temperature (T_b) and the normalized radar cross-section (σ°) are excellent tools for estimating melt duration and extent. The introduction of even small amounts of liquid water into the snow pack dramatically impacts the electrical properties of the snow at microwave frequencies. This results in large changes in the microwave measurements of the surface, enabling melt detection. Current satellites measuring σ° and T_b provide coverage of the complete ice-sheet at least twice daily.

*Corresponding author. Email: long@ee.byu.edu

International Journal of Remote Sensing
ISSN 0143-1161 print/ISSN 1366-5901 online © 2006 Taylor & Francis
http://www.tandf.co.uk/journals
DOI: 10.1080/01431160500534465

Microwave measurements have been successfully used in multiple studies to detect melt duration and extent over Greenland. A single channel threshold has been used with T_b by Mote *et al.* (1993) and Mote and Anderson (1995), and with σ° by Ashcraft and Long (2000) and Wismann (2000). Abdalati and Steffen (1995, 1997a,b, 2001) used a frequency/polarization combination of T_b to detect melt, and Nghiem *et al.* (2001) used the diurnal variability in σ° to detect melt.

Although various methods have been used to detect Greenland melt, there has been no large-scale comparison between these methods. Our object is to provide an inter-comparison between existing methods as well as to introduce a new method for melt detection. This is accomplished by comparing the melt duration and extent obtained from various melt detection methods and sensor combinations. The differences and similarities are discussed in light of the theoretical differences between the various methods and the differences in sensitivity to melt between sensors.

This paper is organized as follows: Section 2 gives a short background on the Greenland ice-sheet and the sensors and data sets. This includes a discussion on the data processing method used to obtain estimates of T_b and σ° on a regularly spaced grid at regular intervals in time. Section 3 introduces a simple model for a melt event and the effects of melt on T_b and σ°. In Section 4, this model is employed to formulate methods to detect melt using T_b and σ°. Selected melt detection methods from other papers are also briefly introduced. Section 5 presents a comparison between various melt detection methods accompanied by a discussion of the observed and theoretical differences and similarities between the various melt detection methods. Section 6 contains a summary and conclusions.

2. Background

Based on the summer melt extent and intensity, the Greenland ice-sheet is divided into four *facies* or *zones* (Benson, 1962). The dry snow zone is the central region of Greenland which experiences negligible melt. Down-slope from the dry snow zone is the percolation zone that experiences some degree of melt, but not to the point of saturation of the previous winter accumulation. Down-slope from the percolation facies is the soaked or wet snow facies where the previous year's accumulation becomes water saturated during the melt period. The lower boundary of the wet snow zone is the firn line, below which is the ablation zone where the previous year's accumulation completely melts during the summer leaving a surface of bare glacial ice and rock.

The T_b data used in this study is from the Special Sensor Microwave Imager (SSM/I). SSM/I measures T_b at seven different frequency polarization combinations. Multiple SSM/I instruments have been flown as part of the Defense Meteorological Satellite Program covering the period from 1988 to the present. Here we use measurements from 19.35 GHz vertical and horizontal polarized channels (19V and 19H) and the 37.0 GHz vertical polarization (37V) channel from the SSM/I instrument aboard the F-14 satellite.

We use σ° measurements from NASA's SeaWinds on QuikSCAT (QSCAT) and the European Remote Sensing satellite (ERS) Advanced Microwave Instrument in scatterometer mode. QSCAT operates at 13.4 GHz and measures σ° at both vertical and horizontal polarizations. We use the vertical polarization data which has an incidence angle of $\sim 56.1^\circ$. QSCAT was launched in June of 1999 and has operated continually since that time. ERS operates at 5.3 GHz measuring σ° at vertical

polarization only. We normalize the ERS σ° measurements to 40° incidence angle. (This normalization is discussed further in Section 4.1.2.) ERS raw σ° measurements are available from two satellites spanning from 1992 to early 2001.

In order to compare the measurements from the different sensors, the raw T_b and σ° data are processed to obtain estimates regularly sampled in space and time. The measurements are interpolated at time τ using the weighted average

$$x(\tau) = \frac{\sum_{i=1}^{N} x_i w(\tau, t_i)}{\sum_{i=1}^{N} w(\tau, t_i)} \tag{1}$$

where N is the number of measurements (x) within a 25 km radius of the point of interest and

$$w(\tau, t_i) = \begin{cases} e^{-\frac{1}{2}(t_i-\tau)^2/\sigma_t^2} & \text{if } |t_i-\tau| < \Delta t_{\max}, \\ 0 & \text{if } |t_i-\tau| \geq \Delta t_{\max}. \end{cases} \tag{2}$$

Estimates are obtained on a 8.9 km spaced grid. For SSM/I and QSCAT the temporal interpolation parameters are $\sigma_t = 6$ hours and $\Delta t_{\max} = 2$ days. For ERS the parameters are $\sigma_t = 24$ hours and $\Delta t_{\max} = 8$ days. The relatively large values for $\Delta t_{\max}$ allow for interpolation over days with missed coverage.

Each sensor samples Greenland at different times of day (see figure 1). To mitigate the effects of the difference in sampling time on melt detection comparison, we compare σ° and T_b estimates at 18:00 local time each day which is near a peak in the time sampling distribution for each sensor. Because the peak sample time for ERS (21:30 local time) is later in the evening past the peak melt, it is expected that ERS will detect less melt than the other sensors.

SSM/I and QSCAT provide complete coverage of the ice-sheet twice daily. ERS requires three days for complete coverage because its swath is narrower. Although ERS requires three days to completely cover the ice-sheet, it covers approximately 80% of the ice-sheet daily making one-day resolution possible over much of the ice-sheet.

3. Theory

In this paper we compare several melt detection methods. The general concept of microwave detection of melt is the same for different methods; however the

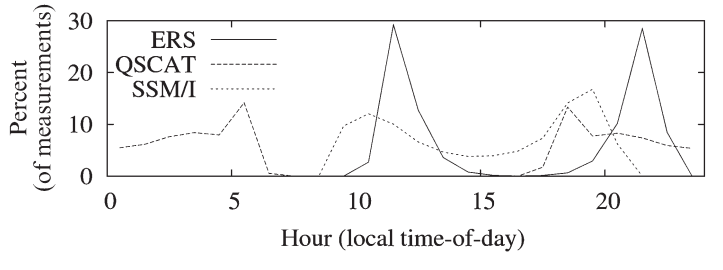

Figure 1. Percent of measurements occurring at the indicated time of day for the various sensors. For melt detection, T_b and σ° are estimated at 18:00 which is close to the maximum sampling for both QSCAT and SSM/I. The peak in the ERS samples is a few hours later in the evening, but is still relatively close to the estimation time.

application of the theory varies. The theory related to melt detection is presented by first providing an overview of the sensitivity of T_b and σ° to melt and then addressing the application of the theory specific to each method.

Microwave measurements are very sensitive to the introduction of liquid moisture into the snow-pack. The most significant change in the electromagnetic properties is a large increase in the imaginary part of the dielectric constant (ϵ''). The introduction of only 0.5% liquid moisture content can increase ϵ'' by over an order of magnitude (Ulaby *et al.*, 1986b). This increases absorption and reduces the penetration depth. The net result of melt is a large decrease in σ° and a large increase in T_b (see figure 2).

3.1 *Melt event model*

The progress of a snow-pack from a frozen state to one where melt is present is a continuous process in which the dividing point between freezing and melting is not well defined. The degree of melt is indicated by the percent liquid moisture content (m_v) of the snow. In this work a melt event is defined based on a m_v threshold and a minimum depth (d) of wet snow. The surface is classified as melting when m_v in the top layer of depth d of snow exceeds some threshold. A simple physical model is

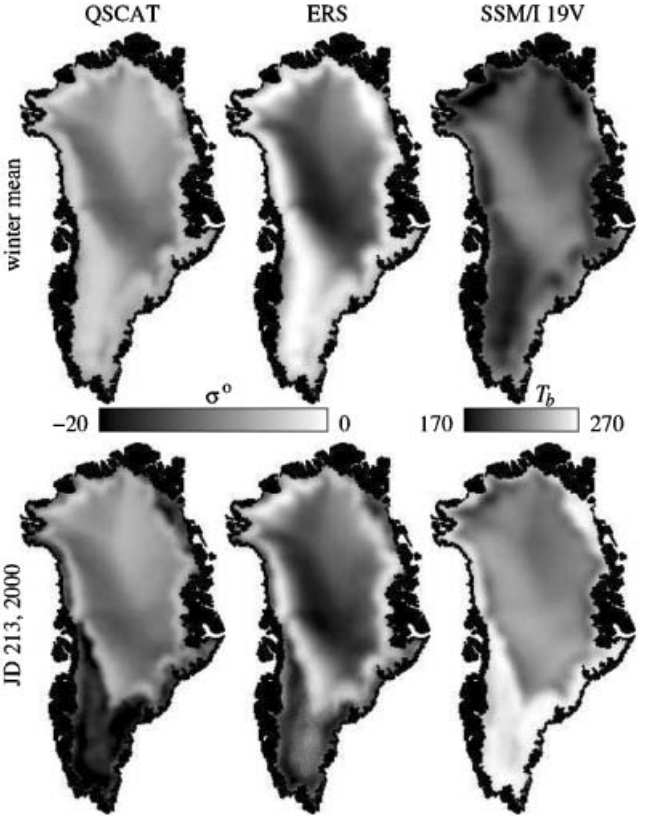

Figure 2. Images of QSCAT σ°, ERS σ° normalized to 40° incidence angle, and SSM/I 19.35 GHz vertical polarization T_b. Top: images of the winter mean using data from December 1, 1999 to February 28, 2000. These winter mean images are the estimates of $\sigma^\circ_{\text{dry}}$ and T_b^{dry} used in the implementation of α-based melt detection. Bottom: images of σ° and T_b estimates on day 213, 2000, a day with intense melt.

employed to relate this definition of melt to a T_b and a σ° threshold for melt detection.

In our simple physical model of a melt event we assume at the melt onset that a uniform layer of wet snow with depth d lies over an infinite half space of dry snow or ice (see figure 3). A model for the brightness temperature radiating from the air/snow boundary in terms of the brightness temperature at a point on the wet/dry snow boundary ($T_b(d)$) is (Ulaby *et al.*, 1986a, p. 216)

$$T_b(0) = T_b(d)e^{-\tau(0,\,d)} + \int_0^d [\kappa_a(z)T_{\text{wet}}(z) + \kappa_s(z)T_{\text{sc}}(z)]e^{-\tau(0,\,z)}\sec\theta(z)\mathrm{d}z \tag{3}$$

where

κ_a –absorption loss coefficient,
κ_s –scattering loss coefficient,
κ_e –extinction coefficient ($\kappa_a+\kappa_s$),
T_{wet} –wet snow physical temperature,
T_{sc} –scattered radiometric temperature,
$\tau(z_1, z_2)$ –optical length ($\int_{z_1}^{z_2}\kappa_e(z)\sec(\theta(z)\mathrm{d}z)$), and
$\theta(z)$ –transmission angle at depth z.

Assuming the wet snow layer is uniform in all significant respects, equation (3) can be rewritten

$$T_b(0) = T_b(d)e^{-\kappa_a^{\text{wet}}\,d\,\sec\theta_{\text{ws}}} + \frac{\kappa_a^{\text{wet}}}{\kappa_e^{\text{wet}}}\left(1-e^{-\kappa_e^{\text{wet}}\,d\,\sec\theta_{\text{ws}}}\right)T_{\text{wet}} + \int_0^d \kappa_s(z)T_{\text{sc}}(z)e^{-\tau(0,\,z)}\sec\theta(z)\mathrm{d}r' \tag{4}$$

where θ_{ws} is the transmission angle through the wet snow. In wet snow, absorption loss dominates over scattering, so $\kappa_a^{\text{wet}} \gg \kappa_s^{\text{wet}}$ and $\kappa_e^{\text{wet}} \approx \kappa_a^{\text{wet}}$. Assuming the contribution from multiple scattering (T_{sc}) is negligible, equation (4) becomes

$$T_b(0) = \alpha T_b^{\text{dry}} + (1-\alpha)T_{\text{wet}} \tag{5}$$

where $\alpha = e^{-\kappa_a\,d\,\sec\theta_{\text{ws}}}$. Based on this model, T_b asymptotically approaches T_{wet} with increasing thickness of the wet snow layer.

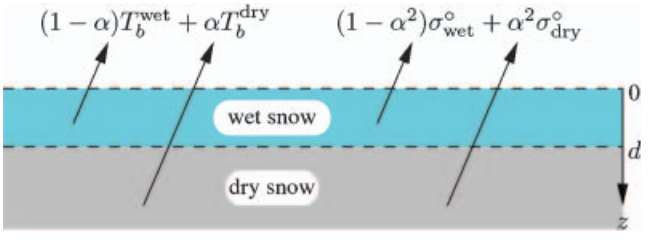

Figure 3. Simplified physical model of a melting surface. The composite T_b of the surface includes the emission from the wet snow and the emission from the dry snow attenuated by the wet snow layer. The composite backscatter is similarly a contribution from the wet snow and an attenuated contribution from the subsurface frozen snow.

In this brightness temperature model we ignore reflections at the air/wet snow boundary and the wet/dry snow boundary. Reflections at the air/snow interface are ignored for SSM/I vertical polarization because the measured emission is near the Brewster angle. Reflections at the wet/dry snow interface are minimal due to the similarity in the magnitude of the dielectric constants in the two media (~3% difference in magnitude based on 1% liquid moisture content in the snow). The primary difference in the electrical properties of the wet and dry snow is in the imaginary part of the dielectric constant. However, the imaginary part is much smaller than the real part, so the difference in the imaginary parts does not significantly affect the magnitude of the dielectric constant.

To estimate the effect of melt on σ°, we model the volume backscatter from the snow as

$$\sigma^\circ = \int_0^\infty \gamma(z) e^{-2\tau(0,\,z)} \sec\theta(z)\,\mathrm{d}z \tag{6}$$

where $\gamma(z)$ represents the normalized backscatter from a layer at depth z with thickness $\mathrm{d}z$. By separating the integral into the contribution from the wet snow and the contribution from the dry snow, we can rewrite equation (6) as

$$\sigma^\circ = \alpha^2 \sigma^\circ_{\mathrm{dry}} + \left(1-\alpha^2\right)\sigma^\circ_{\mathrm{wet}} \tag{7}$$

where

$$\begin{aligned}
\sigma^\circ_{\mathrm{dry}} &= \int_d^\infty \gamma(z) e^{-2\tau(d,\,z)} \sec\theta(z)\,\mathrm{d}z, \\
\sigma^\circ_{\mathrm{wet}} &= \int_d^\infty \gamma_{\mathrm{wet}}\, e^{-2\kappa_e^{\mathrm{wet}} z \sec\theta_{\mathrm{ws}}}\,\mathrm{d}z \\
&= \frac{\gamma_{\mathrm{wet}}}{2\kappa_e^{\mathrm{wet}}},
\end{aligned} \tag{8}$$

and α is defined as in the T_b model. In this equation $\sigma^\circ_{\mathrm{dry}}$ represents the dry snow backscatter without the overlying wet snow layer, and $\sigma^\circ_{\mathrm{wet}}$ represents the volume backscatter from an infinite half-space of wet snow. Note that for backscatter, α is squared due to the two-way attenuation through the wet snow layer. Just as with the T_b model, surface reflections at the air/snow and wet snow/dry snow boundaries are ignored, which is appropriate for vertical polarization. Surface scattering from subsurface layer interfaces (which may be significant) is included in the bulk scattering described by $\sigma^\circ_{\mathrm{dry}}$.

To obtain κ_a^{wet} we estimate the bulk relative dielectric constant (ε_r) of the wet snow layer using the method presented in Ulaby *et al.* (1986c, p. 2072). The wet snow is assumed to have a liquid moisture content $m_v = 1\%$, which matches the value used by Abdalati and Steffen (1997a). A density of $\rho = 0.4\,\mathrm{g/cm^3}$ is assumed, which is consistent with observations of Greenland snow (Benson, 1962). The absorption coefficient is

$$\kappa_a = 2\frac{2\pi f}{c}\Im\{\sqrt{\epsilon_r}\} \tag{9}$$

where f is the frequency, c is the speed of light in a vacuum, and $\Im\{\cdot\}$ represents the imaginary part. We also calculate the power transmission coefficient (Υ) for vertical

Table 1. Calculated wet snow electrical properties corresponding to the three sensors. The air/snow power transmissivity (Υ) is shown for vertical polarization only and is near unity, indicating minimal surface scattering.

Sensor	ERS	QSCAT	SSM/I
frequency	5.3 GHz	13.4 GHz	19.35 GHz
incidence angle	~40	56	53.1
ϵ_r	$1.81 + i0.032$	$1.77 + i0.034$	$1.44 + i0.029$
κ_a (Np/m)	2.63	7.14	9.74
Υ	0.994	0.999	1.000

polarization across the air/wet snow boundary using ϵ_r based on Fresnel reflection. The values of ϵ_r, κ_a and Υ for each of the sensors are listed in table 1.

4. Melt detection methods

We compare results of various melt detection methods over Greenland for the year 2000. A primary goal of this comparison is to inter-relate the spatial and temporal consistency of the individual methods. Additionally, this comparison serves as a cross-validation for the individual melt detection approaches using independent estimates of the daily melt extent. This validation is important because *in situ* validation of large-scale melt detection is difficult due to the limited amount of data available. Our comparison includes six different approaches: Three are based on T_b measurements from SSM/I, and the other three use σ° measurements from ERS and QSCAT.

In general, melt detection for each method is based on thresholding some melt signal ($q(t)$) which varies with time. Let $m(t)$ represent the melt detection with $m=1$ indicating melt and $m=0$ indicating non-melt, i.e.

$$m(t) = \begin{cases} 1 \text{ if } q(t) \geq q_0 \\ 0 \text{ if } q(t) < q_0. \end{cases} \tag{10}$$

Each method is composed of two parts: the definition for $q(t)$ and a constant threshold q_0.

4.1 α-*based methods*

The simplified melt event model introduced in Section 3.1, along with equations (5) and (7), is used as a basis for melt detection using QSCAT, ERS and SSM/I measurements. This is termed α-based melt detection because the threshold is based on the attenuation in the wet snow layer, α. The details of the implementation of α-based melt detection for the different sensors, including the definition for q and the value of q_0, are discussed below.

4.1.1 QSCAT. QSCAT measurements have been used in few studies detecting melt extent and duration over Greenland. We initially used a method based on the mean and standard deviation of σ° during the winter where a drop in σ° of eight winter standard deviations below the winter mean indicates a melt (Ashcraft and Long, 2000). Nghiem *et al.* (2001) also use QSCAT to detect melt over Greenland. Their method is based on the diurnal variability and is discussed in more detail later.

In this paper we present a method for melt detection using QSCAT and the simple melt model presented in the previous section. We term this the Q-α method. A

similar method was employed by Wismann (2000) for melt detection using ERS measurements.

Recalling that $\sigma^{\circ}_{\text{wet}}$ is relatively small (typically over 10 dB below $\sigma^{\circ}_{\text{dry}}$), the contribution from the $(1-\alpha^2)\sigma^{\circ}_{\text{wet}}$ term in equation (7) is assumed negligible. In this case, melt is indicated by

$$\sigma^{\circ} < \alpha^2 \sigma^{\circ}_{\text{dry}} \tag{11}$$

which in dB is written

$$\sigma^{\circ} < \sigma^{\circ}_{\text{dry}} + 2{\cdot}10 \log_{10}\alpha. \tag{12}$$

Formulated in terms of q and q_0, the definitions are

$$q(t) = \sigma^{\circ}_{\text{dry}} - \sigma^{\circ}(t) \quad \text{(in dB)} \tag{13}$$

with $q_0 = 2{\cdot}10\log_{10}\alpha$.

In this method, the signal $q(t)$ represents the deviation in σ° from the backscatter from a dry snow surface. Because σ° is relatively constant during the non-melt period, we can estimate $\sigma^{\circ}_{\text{dry}}$ as the average over the winter period when no melt is expected to occur. In general, $\sigma^{\circ}_{\text{dry}}$ is a function of the observation geometry including the incidence angle (θ) and the azimuth angle (ϕ). Additionally, it is dependent on the offset (**r**) of the measurement centroid from the estimation point of the average σ°. To estimate these dependencies, we use the method from Ashcraft and Long (2004):

$$\sigma^{\circ}(\phi, \mathbf{r}) = A + M_1 \cos(\phi - \phi_1) + M_2 \cos(2\phi - \phi_2) + s(\mathbf{r}\cdot\hat{\mathbf{g}}) \tag{14}$$

where the model parameters A, M_1, ϕ_1, M_2, ϕ_2, s, and $\hat{\mathbf{g}}$ are obtained through linear least-squares regression. Because of the narrow incidence angle sampling by QSCAT, incidence angle dependence is ignored.

The model parameters are estimated using three months of QSCAT data from December 1, 1999 to February 28, 2000. Variations from the winter average are estimated as

$$q(t_i) = \sigma^{\circ}(\phi_i, \mathbf{r}_i) - \sigma^{\circ}_i. \tag{15}$$

where i indicates the measurement index. We use the temporal interpolation discussed in Section 2 to estimate q at 18:00 local time each day. For the threshold for Q-α melt detection we set $q_0 = 3$ dB. This corresponds to a layer of wet snow with 3.8 cm depth and $m_v = 1.0\%$.

4.1.2 ERS. Melt detection using ERS, termed E-α melt detection, is similar to the Q-α method and the method used by Wismann (2000) to estimate melt using ERS. The differences between these methods are in the details of the data processing and the threshold selection.

ERS has a broad sampling in incidence angle (θ), so θ dependence is included in the model such that

$$\begin{aligned}\sigma^{\circ}(\theta, \phi, \mathbf{r}) = A + B_1(\theta - 40) + B_2(\theta - 40)^2 + s(\mathbf{r}\cdot\hat{\mathbf{g}}) \\ + M_1 \cos(\phi - \phi_1) + M_2 \cos(2\phi - \phi_2)\end{aligned}$$

where θ is in degrees. The model parameters are estimated using ERS data from December 1, 1999 to February 28, 2000. Estimation and re-sampling of q is

performed using the same procedure as in Q-α, with the only difference being the inclusion of the incidence angle dependence and different temporal interpolation parameters as discussed in Section 2.

ERS σ° measurements are less sensitive to liquid water in the snow than the QSCAT σ° measurements. The lower frequency of ERS (5.3 GHz) compared to QSCAT (13.4 GHz) results in less absorption by a layer of wet snow with the same depth and moisture content. Thus, for an equivalent theoretical melt definition, the ERS threshold (q_0=1.0 dB) is much smaller than for QSCAT. This small threshold can create excessive false alarms due to variance in the q estimates and other processes which effect the backscatter.

To avoid this false-alarm problem and improve the consistency between Q-α and E-α, we adopt a different, empirical method to select a threshold, q_0. We approximate the distribution of q during melt ($p(q|m=1)$) and the distribution of q during non-melt ($p(q|m=1)$) for E-α using the classification results from Q-α melt detection. We then minimize the probability of detection error using the maximum a posteriori (MAP) criteria

$$\hat{m}(t) = \begin{cases} 1 & \text{if } \frac{p(q(t)|m=1)p(m=1)}{p(q(t)|m=0)p(m=0)} > 1 \\ 0 & \text{otherwise} \end{cases} \tag{16}$$

where $\hat{m}(t)$ is the E-α melt estimate and $p(m)$ is the probability of melt or non-melt inferred from Q-α melt detection during 2000. The probability densities are shown in figure 4. The MAP threshold is at the intersection of the two densities at q_0=2.7 dB.

There is a difference between the E-α melt detection and that of Wismann (2000) in the method of normalizing σ° based on the observation geometry. Instead of re-estimating the observation geometry dependence with each new normalized σ° estimate, the E-α method assumes that the dependence on observation geometry is constant during the full melt season. This assumption enables increased temporal resolution and reduced variance in the melt signal (Ashcraft and Long, 2004). There is also a small difference in the threshold with q_0=2.8 dB used for E-α and q_0=3.0 dB to equivalent to the threshold used by Wismann.

4.1.3 SSM/I. SSM/I T_b measurements have been used in various studies to detect melt over Greenland. Two methods are used in the melt detection inter-comparison. Prior to discussing these two methods, we introduce a new α-based T_b melt detection method.

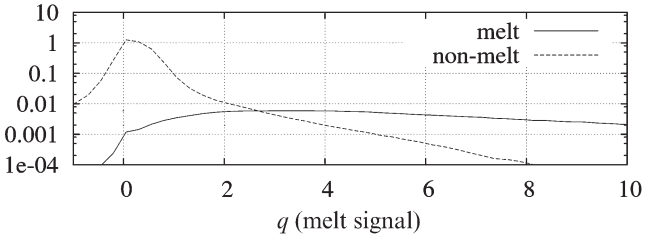

Figure 4. Normalized histogram of the ERS melt signal, q, for melt ($p(q|m=1)p(m=1)$) and non-melt ($p(q|m=0)p(m=0)$). The classification of melt or non-melt is based on the results of Q-α melt detection. The intersection of the two densities at 2.8 dB is the minimum error threshold for ERS melt detection based on the MAP criteria.

For α-based melt detection with SSM/I we use the 19V channel. The 19.35 GHz frequency is chosen because it is the closest SSM/I frequency to that of QSCAT and ERS. Vertical polarization is chosen to minimize the impact of layer interfaces as discussed in Section 3. Based on equation (5), a melt is indicated by

$$T_b > \alpha T_b^{\mathrm{dry}} + (1-\alpha) T_{\mathrm{wet}} \tag{17}$$

where the value of α is determined by the thickness of the wet snow layer. This detection can be written in terms of $q(t)$ as

$$q(t) = \frac{T_b(t) - T_b^{\mathrm{dry}}}{T_{\mathrm{wet}} - T_b^{\mathrm{dry}}} \tag{18}$$

and $q_0 = 1-\alpha$.

Melt detection requires an estimate of T_{wet} and T_b^{dry}. We assume that the wet snow-pack is at approximately melting temperature ($T_{\mathrm{wet}} \approx 273$ K). A precise estimate of T_b^{dry} is difficult to obtain. This is primarily due to the variability and uncertainty in the snow temperature throughout the year. For the purpose of simplicity, in this paper T_b^{dry} is estimated as the average T_b from December 1 to February 28 during the previous winter at each location. This is expected to be reasonably close to T_b^{dry}, although biased somewhat low.

Due to the uncertainties in the estimation of T_b^{dry} we use an empirical method to obtain an estimate of q_0 that is similar to the method used for E-α. Figure 5 shows the histogram of SSM/I q values for melt and non-melt based on the results from the Q-α melt detection. The threshold based on the MAP criteria is $q_0 = 0.47$, the intersection of the two histograms. This threshold is equivalent to a theoretical wet snow layer depth of 4.7 cm with $m_v = 1.0\%$.

4.2 T_b-M

Another method using the SSM/I 19V channel, termed the T_b-M method, originates from Mote *et al.* (1993). Based on this method, a rise in T_b to over 31 K above winter mean T_b indicates melt. Interpreting the winter mean T_b as an estimate of T_b^{dry} as in the previous method, a melt is indicated by

$$T_b > T_b^{\mathrm{dry}} + 31. \tag{19}$$

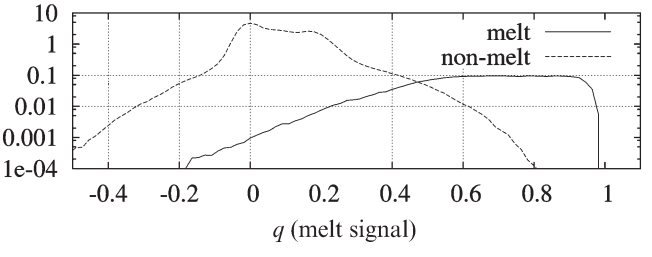

Figure 5. Normalized histogram of the SSM/I melt signal q for melt and non-melt. The classification as melt or non-melt is based on melt detection results from the Q-α method. The intersection of the two densities at 0.46 represents the minimum error threshold for SSM/I melt detection based on the MAP criteria.

The corresponding definitions for q and q_0 are

$$q(t) = T_b(t) - T_b^{\mathrm{dry}} \tag{20}$$

and $q_0 = 31$ K. Just as in the previous method, T_b^{dry} is estimated to be the mean T_b between December 1, 1999 and February 28, 2000 at each location.

4.3 *XPGR*

The final T_b method compared is the cross-gradient polarization ratio (XPGR) from Abdalati and Steffen (1995, 1997a,b, 2001). This method employs the differences between the SSM/I 19H and 37V channels to detect melt. For this method,

$$q(t) = \mathrm{XPGR} = \frac{T_b^{19\mathrm{H}}(t) - T_b^{37\mathrm{V}}(t)}{T_b^{19\mathrm{H}}(t) + T_b^{37\mathrm{V}}(t)} \tag{21}$$

and $q_0 = -0.0158$ (Abdalati and Steffen, 1997a). An equivalent criterion is if the observed ratio $T_b(19\mathrm{H})/T_b(37\mathrm{V})$ is greater than the constant value $(1+q_0)/(1-q_0)$ the surface is flagged as melting. Based on the Rayleigh–Jeans approximation ($T_b = eT$), the temperature cancels and the criterion becomes a threshold on the ratio of the emissivity at the two frequencies and polarizations. A significant advantage of this method is that $q(t)$ does not depend on estimates of any physical surface parameters.

4.4 *Q-DV*

The final method employed in our comparison is based on the diurnal variation in σ° observed by QSCAT (Nghiem *et al.*, 2001). We term this the Q-DV method. The melt criterion for Q-DV is that a diurnal change greater than 1.8 dB indicates melt. To determine the diurnal variation we use estimates of σ° at 6:00 and 18:00 local time for QSCAT. In terms of $q(t)$ and q_0, this method is

$$q(t) = \left|\sigma^\circ_{18:00}(t) - \sigma^\circ_{6:00}(t)\right| \tag{22}$$

where t is constrained to be discrete at one day sampling and $q_0 = 1.8$ dB. This method is not used with ERS because of inadequate temporal resolution.

5. Method comparison

These six methods (Q-α, E-α, T_b-α, T_b-M, XPGR, Q-DV) are compared based on the detected melt for each day during the year 2000. Metrics for this comparison include the total melt (M), the melt extent (E), and the daily melt extent (ξ). The method differences are illustrated using images of the melt duration, melt extent, and temporal variation.

The total melt and the melt extent detected by each method are listed in table 2. The total melt is given by

$$M = a \sum_{t=1}^{365} \sum_{i=1}^{N} m_i(d) \tag{23}$$

where a is the area of a single pixel ($8.9^2\,\mathrm{km}^2$), t is the day of the year, i is the pixel index, and N is the total number of pixels. The three α-based methods and the T_b-M method result in similar estimates of M, approximately double that of the Q-DV and XPGR methods. The two QSCAT methods result in the high and low extremes

Table 2. Total melt ($km^2 days \times 10^6$) and melt extent ($km^2 \times 10^4$) detected by the different methods for 2000. The bottom row lists the percent of the ice-sheet the melt extent covers.

	Q-α	E-α	T_b-α	T_b-M	XPGR	Q-DV
total melt (M)	30.3	28.2	28.6	27.3	14.6	12.2
melt extent (E)	95.9	79.3	101.9	99.2	52.9	97.2
percent	58	48	62	60	32	59

in the total melt detection with the Q-α method detecting the largest amount and the Q-DV method detecting the smallest.

The melt extent,

$$E = a \sum_{i=1}^{N} \max_{t} m_i(t), \tag{24}$$

is consistent between the methods with the exception of XPGR which detects just over half of the melt area of the others and E-α which detects about 80% of the areal melt extent of the others. To determine the percentage of the ice-sheet experiencing melt, we divide the melt extent by the total area within the ice-sheet mask. Four of the six methods estimate that about 60% of the ice-sheet experiences melt. This is consistent with the estimated dry snow extent from Benson (1962). Based on Benson's definition of the dry snow zone and the ice-sheet mask used herein, 60% of the ice-sheet experiences melt in a typical year.

Additional insights into the differences between the individual methods are gained by comparing the variation in daily estimates of the daily melt extent

$$\xi(t) = \sum_{i=1}^{N} m_i(t). \tag{25}$$

The variations in $\xi(t)$ for the different methods are shown in figure 6. The T_b-α and T_b-M methods give consistent estimates of $\xi(t)$. The XPGR method is biased low during periods of melt onset and peak melt. XPGR indicates very little melt around day 213 when the other methods detect the maximum melt extent. During the refreeze period (after day 235), XPGR exceeds the estimated melt extent of the other methods.

For the σ° methods, E-α and Q-α result in similar $\xi(t)$ estimates with the E-α method having a small negative bias at melt onset and peak melt times, and a small positive bias during the refreeze period. Q-DV is consistently biased low, estimating approximately 50% of the melt area of other methods. The peaks in the Q-DV $\xi(t)$ estimates occur just prior to the peaks in the other methods.

Direct comparison between the $\xi(t)$ estimates from the T_b-α and Q-α methods shows very close agreement. The difference between the two is a larger estimate of the melt extent from T_b-α during melt onset and a larger extent estimate by Q-α during periods of refreeze. This is attributed to a difference in the sensitivity to melt due to the frequency difference which is discussed in Section 5.1.

Figure 7 includes images illustrating the annual melt extent, the annual melt duration, and the temporal/spatial variation of the detected melt for summer 2000. The melt duration for each method is illustrated by comparing the melt duration estimated by each individual method with the average melt duration estimated by the α-based methods. The melt duration detected by the Q-α method is about

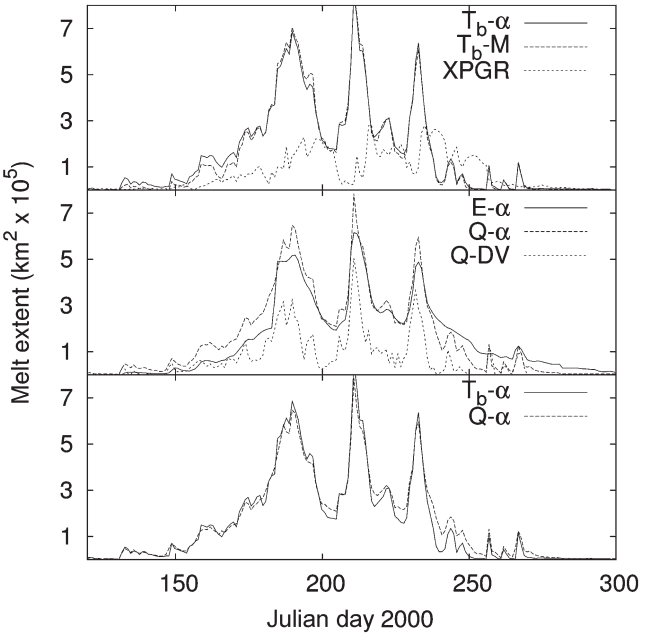

Figure 6. Melt extent each day as observed by the different methods. The top plot shows a comparison between T_b methods, the middle plot shows comparisons between σ° methods, and the bottom plot shows the comparison between a single T_b and single σ° method.

average over the annual melt extent. E-α estimates of the duration are above average in regions with a long average melt duration. T_b-α melt duration estimates are below average in the same regions. The difference between the T_b-M melt duration estimates and the α-based average varies by region. A general trend is observed of above average estimates in areas with low winter values and below average estimates in regions with high winter T_b values (see figure 2 for a winter T_b image).

In general, XPGR and Q-DV detect shorter melt than the α-based methods. However, for Q-DV this is only true for lower elevations: at higher elevations the melt duration is very close to the estimates of the α-based methods. With XPGR, exceptions exist on the east side of the ice-sheet around 64° N and 77° N where XPGR detects longer melt than the α-based methods.

The middle row of images in figure 7 shows a comparison between the melt extent obtained from the individual methods and the melt extent obtained by combining the methods. Just as indicated in table 2, the Q-α, T_b-α, T_b-M, and Q-DV methods agree closely on the extent of the melt. Differences are primarily on the border of the dry snow zone and are attributed to small differences in the definition of melt intrinsic to each method. For E-α and XPGR, areas of missed melt detection are in the upper regions of the percolation zone, indicating that these methods are less sensitive to small amounts of melt.

The bottom row in figure 7 is a set of Hovmöller diagrams that illustrates the changes in the melt extent over time along a transect across the southern portion of the ice-sheet. These images aid in understanding the spatial and temporal consistency in the melt detection methods.

The α-based methods all appear to be spatial and temporally consistent with expected trends in the summer melt process. Melt, as a function of time, begins at

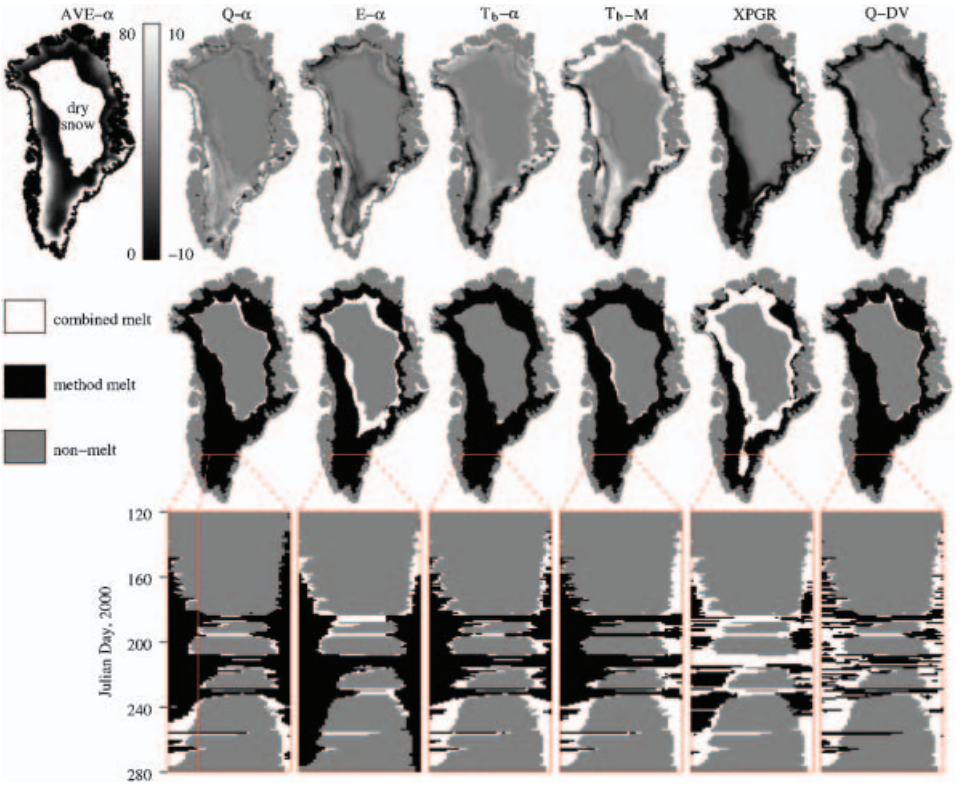

Figure 7. Top row: (left) Average melt duration in days obtained from the α-based methods. (right) Images of the difference between each method and the α-based average. Middle row: Annual melt extent from the individual methods compared with the annual melt extent combining all methods. Bottom row: Hovmöller diagrams showing the variation in the melt extent over time along a transect across the southern portion of the ice-sheet as indicated in the figure. In the bottom two rows, white represents the area that is designated as melting by any of the methods. Black is imposed over the white to indicate the melt area detected by the method specified in the column header. Gray is non-melt area. The line over the Q-α Hovmöller diagram indicates the location for the Q versus t plots in figure 8.

the edges and progresses toward the interior of the ice-sheet. Increases and decreases in the melt extent occur gradually over time. Near the peak melt period, where the upper extent of the melt is near the crest of the ice-sheet, the changes in the melt extent occur more rapidly. This increased rate of change in melt area is attributed to the small slope of the ice-sheet near the crest resulting in large changes in the areal extent of the melt due to small changes in temperature. It appears that a warm front moved across the ice-sheet near day 255 causing a short melt event. This is detected by the Q-α and T_b-α methods, but not by the E-α method. The missed detection by E-α is attributed to the lower temporal resolution of the ERS data and to the ERS local time sampling. The temporal resolution of ERS, along with the differences in melt detection by the α-based methods, are discussed in Section 5.1.

On the west side of the ice-sheet, the Hovmöller diagram for the T_b-M method is similar to those for the α-based methods. The melt detected by T_b-M and T_b-α is almost identical, with T_b-M detecting the upper extent of the melt about 10–20 km further up-slope. On the east, however, there is a notable difference: the T_b-M

method detects less melt than the α-based methods, and melt is only detected during intense melt periods.

Substantial differences are also observed in the Hovmöller diagrams between XPGR and the other melt detection methods. These differences are largest during periods of intense melt based on the results of the α-based and T_b-M methods. An example is observed near day 213, a time when other methods are detecting maximum melt. The XPGR Hovmöller diagram indicates no melt at this time; however, previous to, and after this period, XPGR detects a sizable amount of melt. XPGR also results in short periods of detection of melt at higher elevations while not detecting melt at lower elevations. An example of this is shown in the XPGR Hovmöller diagram near day 235.

Although the maximum melt extent estimates from Q-DV closely match that of other methods, the daily variation in the melt extent detected by Q-DV is very different from that of any other method. Melt detection appears sporadic in both time and space. Melt detection by Q-DV is not accepted as accurate based primarily on the lack of spatial and temporal correlation, making this method inconsistent with the results of the other methods and inconsistent with what is expected for the natural melt progress.

To further illustrate the similarities and differences between the melt detection methods, figure 8 displays $q(t)$ and q_0 for each method at one location. Melt onset is indicated in each plot by an abrupt large increase in $q(t)$. During the melt period, the $q(t)$ signal of the α-based methods and T_b-M are similar. The E-α signal lacks some of the higher frequency components of the other methods due to coarser temporal resolution in the ERS data. The variation in the T_b-α and T_b-M $q(t)$ during non-melt is attributed to temperature variation and accumulation. The XPGR and Q-DV melt signals are substantially different from the other methods. With XPGR, local maxima in $q(t)$ occur at times similar to those observed for the α-based and T_b-M methods; however, the relative amplitude of the peaks are different, contributing to discrepancies in the melt detection by XPGR and the other methods. During the melt period, the Q-DV melt signal is much more variable than the other methods. During non-melt, $q(t)$ remains relatively constant for both XPGR and Q-DV.

To evaluate the agreement between the methods on the location and time of melt, we use the correlation coefficient R. The correlation is calculated based on whether or not melt is detected for individual pixels daily. The correlation between the α-based methods is high, between 0.74 and 0.87, indicating that these methods are consistent in time and location of detected melt. The T_b-M method is also strongly correlated to the α-based methods. XPGR and Q-DV have lower correlations with the other methods, with correlation to the α-based methods ranging from 0.38 to 0.49. The latter two methods also exhibit little correlation with each other having a joint correlation coefficient of only 0.19. The correlation of XPGR with the other methods is maximized by using a XPGR threshold near $q_0 = -0.05$. This change in the threshold increases the correlation with the α-based methods to between 0.46 and 0.54 and the correlation with Q-DV to $R = 0.29$.

5.1 *Discussion*

The differences in the melt detected by the individual methods are attributed to differences in sensitivity to melt due to frequency and/or differences in the definition of melt implicit with each method.

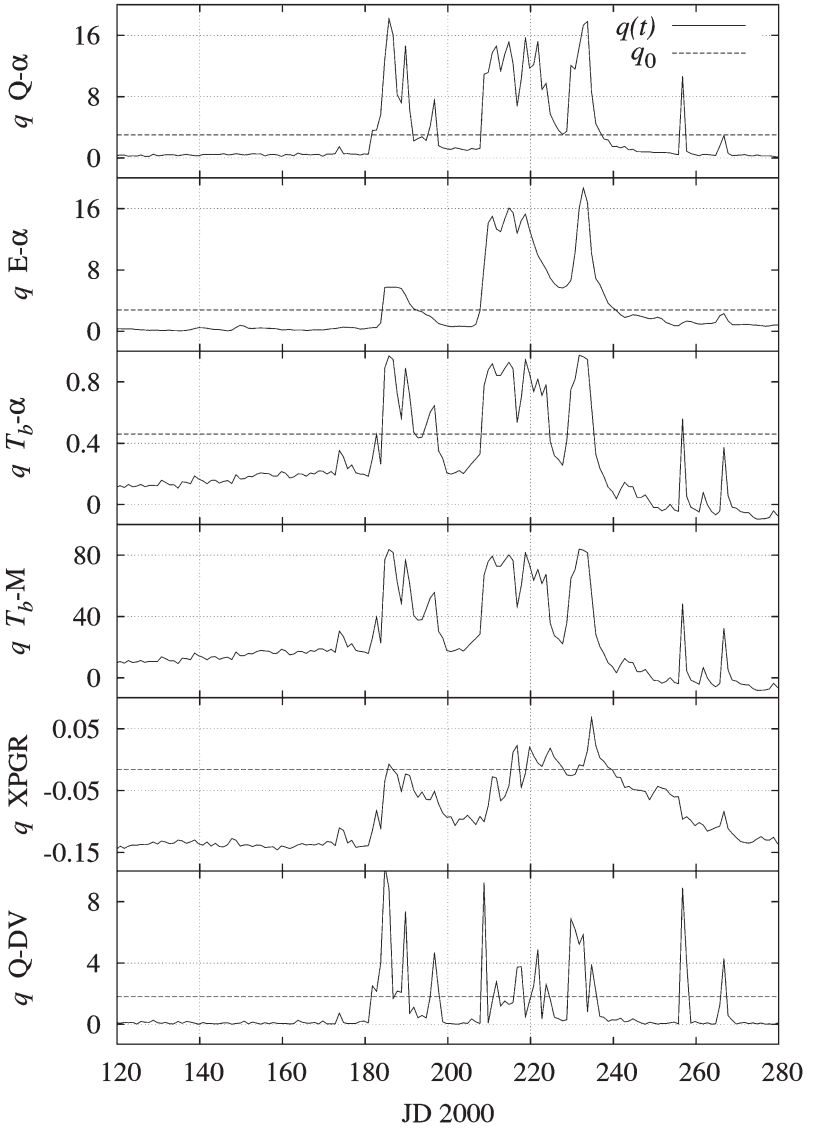

Figure 8. Plots of the melt signal ($q(t)$) for the different melt detection methods at 64.9 N, 47.3 W. The location is indicated in the Q-α Hovmöller diagram in figure 7.

The α-based methods define a melt event based on a uniform wet snow layer with a specified m_v and minimum depth. This property contributes to the spatial and temporal consistency of these methods. It also helps to ensure consistency in the different facies and regions of the ice-sheet. Given a value of α associated with a threshold, a line can be drawn indicating the relationship between m_v and d for melt detection. These lines are shown in figure 9 for the three α-based methods. The thresholds for Q-α and T_b-α are similar, with the small difference representative of the uncertainty in the T_b^{dry} estimates. The E-α minimum wet snow depth for melt detection is about double that of Q-α and T_b-α for any given value of m_v. As discussed in Section 4.1.2, the 5.3 GHz ERS measurements are less sensitive to snow

Table 3. Correlation coefficient (R) between the melt signal ($m_p(d)$) of the various methods.

	Q-α	E-α	T_b-α	T_b-M	XPGR	Q-DV
Q-α	1.00	0.81	0.87	0.78	0.42	0.57
E-α	0.81	1.00	0.74	0.68	0.49	0.44
T_b-α	0.87	0.74	1.00	0.85	0.38	0.55
T_b-M	0.78	0.68	0.85	1.00	0.35	0.54
XPGR	0.42	0.49	0.38	0.35	1.00	0.19
Q-DV	0.57	0.44	0.55	0.54	0.19	1.00

moisture content than the QSCAT and SSM/I measurements. To reduce the false-alarm rate due to noise, the threshold is chosen using an empirical method to match Q-α melt detection rather than using the theoretical equivalent. The empirically chosen threshold, $q_0 = 2.7$ dB, coincides with a theoretical wet layer depth of 10.4 cm. This is more than double the theoretical wet snow depth for Q-α melt detection. Thus, E-α requires a more intense melt before detection occurs. This contributes to E-α generally detecting less melt than the Q-α and T_b-α methods.

Another factor affecting E-α melt detection is the local time of day of the ERS samples. The peak ERS sampling is around 11:30 and 21:30 local time (see figure 1) which is before and after the expected period of peak diurnal melt. This is also expected to reduce the melt detected using E-α.

The discussion thus far has focused primarily on differences in detecting melt at onset, which is the focus of of the α-based melt detection. During refreeze the vertical melt profile can be quite different than that of the simple physical model presented. After an intense melt event, subsurface liquid moisture remains after the refreezing of the surface. Due to the large penetration depth at low frequencies, melt is still detected after surface refreeze. The lingering melt detection after intense melt is observed in the results from E-α in the melt extent plot in figure 6 and the the E-α Hovmöller diagram in figure 7. This is also observed in comparing the Q-α results to those of T_b-α in the same figures.

T_b-M is the non-α method with results most similar to the α-based methods. Melt detection using T_b-M is based on the winter T_b statistics and melt T_b statistics at selected locations with the threshold based on the difference between the winter mean T_b and the mean T_b during a melt period as well as the standard deviation of T_b during the melt period (Mote *et al.*, 1993). Over much of the ice-sheet this method performs very well. However, at locations which have a high winter mean T_b value, this method significantly under-detects the melt. This under-detection can be explained using our simple melt model: In southwest Greenland, the mean winter T_b

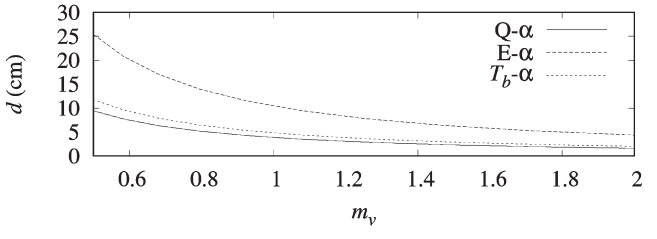

Figure 9. Wet snow percent liquid moisture content (m_v) versus depth (d) corresponding to the melt threshold used in the Q-α, E-α, and T_b-α melt detection methods. The lines are calculated based on a snow density of $\rho = 0.4$ g/cm^3.

is ≈195 K. This results in melt detection for T_b-M when T_b>226 K. The corresponding T_b-α physical model parameters are α=0.60, and d=3.8 cm based on m_v=1.0%. In the southeast, the winter mean is T_b≈230 K resulting in T_b-M melt detection when T_b>261 K. The corresponding T_b-α physical model parameters here are α=0.28 and d=9.6 cm based on m_v=1.0%. Note the difference in the theoretical depth of the wet snow layer associated with the melt detection threshold at the two locations. This theoretical difference wet snow depth is further accentuated by the low bias in the T_b^{dry} estimate, making the actual difference even greater. Hence, T_b-M results in different melt definitions at different locations with an end result of higher sensitivity to melt in the southwest of the ice-sheet than in the southeast. Effects of this regional difference are observed in the limited detection of melt on the east of the ice-sheet in T_b-M melt duration image and the Hovmöller diagram in figure 7. We attribute the cold region bias (more melt detected at a cold location than a warm location), which was also observed by Abdalati and Steffen (1995), to this effect. An alternate method proposed by Mote and Anderson (1995) may reduce the effects of this anomaly; however, this method, which includes inversion of a microwave emission model, is significantly more complex and difficult to reproduce.

The Q-DV method is based on the rapid fluctuation of σ° during a melt event. Because of freezing at night and melting during the day it is assumed that there is a large fluctuation in σ° over the course of a day. The main caveat against this method is that it is based on a sufficient, but not a necessary condition for melt detection. A diurnal change of over 1.8 dB over snow is indicative of melt; however, the converse is not true. The surface can theoretically be melting and have negligible diurnal variation. This is observed in the Q-DV Hovmöller diagram in figure 7 where long periods of melt based on results of other methods are interspersed with intermittent gaps of undetected melt in the Q-DV results.

The XPGR method is based on 19 GHz being more responsive to melt onset in the firn than 37 GHz and a melt producing a larger increase in H-pol emissivity than in V-pol (Abdalati and Steffen, 1997a). However, it appears that significant melt can occur without meeting the XPGR melt detection requirement. An example is observed around day 213 when the other methods detect maximum melt extent, and XPGR detects minimal melt. One attribute of XPGR is that, due to the difference in the penetration depths of the two channels, it detects melt after the surface has refrozen if the subsurface contains liquid moisture (Abdalati and Steffen, 1997a).

6. Summary and conclusions

Melt detection using σ° and T_b is related to snow wetness and the depth of the wet snow layer at melt onset using a simple physical model. The technique for melt detection using σ° is equivalent to a threshold at a fixed value below the winter mean. We use a threshold of 3 dB for QSCAT and 2.7 dB for ERS. Model based melt detection using T_b is only slightly more complex. A melt is indicated by a rise in T_b above some threshold which is a function of the difference between the winter mean T_b and the maximum T_b for wet snow (273 K). The selected threshold is 47% of this difference added to the winter mean T_b. The threshold for QSCAT corresponds to a theoretical wet snow layer with m_v=1.0% and depth d=3.8 cm. An empirical method based on MAP detection and the QSCAT melt detection was used to select the ERS and SSM/I thresholds. The theoretical wet snow depths corresponding to the empirically obtained thresholds are d=10.4 cm for ERS and d=4.8 cm for SSM/I 19V.

Melt detection based on our simple physical model, which we term α-based detection, eliminates unnatural phenomena observed in the results for other melt detection methods. Improvements include similar melt duration estimates for similar elevations on the east and west sides of the ice-sheet, elimination of mid-summer melt detection gaps between periods of intense melt, and the detection of melt at lower elevations before, during, and after detection of melt at higher elevations.

Some differences are observed in α-based melt detection for the three sensors. The E-α method is the most dissimilar, detecting a total melt extent of 48% of the ice-sheet compared with 58% for Q-α and 62% for T_b-α. This difference is attributed to lower temporal resolution, reduced sensitivity to melt due to the lower frequency, and different local time of day sampling for ERS compared with QSCAT and SSM/I. The E-α method also detects above average melt during the refreeze period. This is attributed to the relatively large penetration depth at C-band making the measurements sensitive to the presence of subsurface melt remaining after surface refreeze. This phenomenon of extended melt detection is observed to a smaller degree in QSCAT melt detection when compared with SSM/I and is attributed to a difference in penetration depth due to the frequency difference between the two instruments.

The results for non-α methods are widely variable. Estimates of the melt extent are near 60% of the ice-sheet for T_b-M and Q-DV, which is similar to the Q-α and T_b-α results. XPGR, however, indicates that only 32% of the ice-sheet experienced melt during the summer of 2004. The non-α methods are also generally less correlated with other methods with the lowest correlation R=0.19 between XPGR and Q-DV.

The α-based melt detection is based on a model for melt onset. However, during refreeze the vertical melt profile is potentially quite different from the profile at melt onset. This is especially true in regions with extended melt duration. Although the α-based method performs moderately well in determining refreeze, the relationship between the end of the detected melt and the surface profile is not as well understood as at melt onset. This phenomenon is one reason for the differences between the α-based methods during the refreeze period. We are currently studying ways to improve the characterization of the surface during the refreeze process.

In situ measurements of the vertical wetness profile of the surface would aid in further validating the α-based melt detection. Simultaneous measurements from scatterometer and radiometer instruments aboard the same platform will further enhance the ability to inter-relate T_b and σ° melt detection. This is the setup with SeaWinds and AMSR on ADEOS II.

References

Abdalati, W. and Steffen, K., 1995, Passive microwave-derived snow melt regions on the Greenland ice sheet. *Geophysical Research Letters*, **22**, pp. 787–790.

Abdalati, W. and Steffen, K., 1997a, Snowmelt on the Greenland ice sheet as derived from passive microwave satellite data. *Journal of Climate*, **10**, pp. 165–175.

Abdalati, W. and Steffen, K., 1997b, The apparent effects of the Mt. Pinatubo eruption on the Greenland ice sheet melt extent. *Geophysical Research Letters*, **24**, pp. 1795–1797.

Abdalati, W. and Steffen, K., 2001, Greenland ice sheet melt extent: 1979–1999. *Journal of Geophysical Research*, **106**, pp. 33983–33988.

Ashcraft, I.S. and Long, D.G., 2000, SeaWinds views Greenland. In *Proceedings of the IEEE International Geoscience and Remote Sensing Symposium*, Vol. 3, pp. 1131–1136.

Ashcraft, I.S. and Long, D.G., 2006 (in press), Observation and characterization of radar backscatter over Greenland, submitted to *IEEE Transactions on Geoscience and Remote Sensing*.

BENSON, C.S., 1962, Stratigraphic studies in the snow and firn of the Greenland ice sheet. U.S. *Army Snow Ice and Permafrost Research Establishment*. Available online at: http://www.scp.byu.edu/docs/Benson_report_edit_compressed.pdf.

KRABILL, W., ABDALATI, W., FREDERICK, E., MANIZADE, S., MARTIN, C., SONNTAG, J., SWIFT, R., THOMAS, R., WRIGHT, W. and YUNGEL, J., 2000, Greenland ice sheet: High-elevation balance and peripheral thinning. *Science*, **289**, pp. 428–430.

MOTE, T.L. and ANDERSON, M.R., 1995, Variations in snowpack melt on the Greenland ice sheet based on passive-microwave measurements. *Journal of Glaciology*, **41**, pp. 51–60.

MOTE, T.L., ANDERSON, M.R., KUININEN, K.C. and ROWE, C.M., 1993, Passive microwave-derived spatial and temporal variations of summer melt on the Greenland ice sheet. *Annals of Glaciology*, **17**, pp. 233–238.

NGHIEM, V.S., STEFFEN, K., KWAK, R. and TSAI, W.-Y., 2001, Detection of snowmelt regions on the Greenland ice sheet using diurnal backscatter change. *Journal of Glaciology*, **47**, pp. 539–547.

ULABY, F., MOORE, R. and FUNG, A., 1986a, *Microwave Remote Sensing: Active and Passive*, Vol. 1 (Norwood, Massachusetts: Artech House).

ULABY, F., MOORE, R. and FUNG, A., 1986b, *Microwave Remote Sensing: Active and Passive*, Vol. 2 (Norwood, Massachusetts: Artech House).

ULABY, F., MOORE, R. and FUNG, A., 1986c, *Microwave Remote Sensing: Active and Passive*, Vol. 3 (Norwood, Massachusetts: Artech House).

WISMANN, V., 2000, Monitoring of seasonal snowmelt on Greenland with ERS scatterometer data. *IEEE Transactions on Geoscience and Remote Sensing*, **38**, pp. 1821–1826.